======= PRODUCTION, STRUCTURE, PROPERTIES =======

From Soft to Superhard: Fifty Years of Experiments on Cold-Compressed Graphite

Y. Wang[a] and K. K. M. Lee[b]

[a]*Department of Physics, Oakland University, Rochester, MI 48309, USA*
[b]*Department of Geology & Geophysics, Yale University, New Haven, CT 06511, USA*

Received August 21, 2012

Abstract—In recent years there have been numerous computational studies predicting the nature of cold-compressed graphite yielding a proverbial alphabet soup of carbon structures (e.g., bct-C_4, K_4-, M-, H-, R-, S-, T-, W- and Z-carbon). Although theoretical methods have improved, the inherent nature of graphite (i.e., low-Z) and the subsequent room-temperature, high-pressure phase transition (i.e., low symmetry, nanocrystalline and sluggish), make experimental measurements difficult to execute and interpret even with the current technology of 3rd generation synchrotron sources. The room-temperature, high-pressure phase transition of graphite has been detected by numerous kinds of experiments over the past fifty years, such as electrical resistance measurements, optical microscopy, X-ray diffraction, inelastic X-ray scattering, and Raman spectroscopy. However, the identification and characterization of high-pressure graphite is replete with controversy since its discovery more than fifty years ago. Recent experiments confirm that this phase has a monoclinic structure, consistent with the M-carbon phase predicted by theoretical computations. Meanwhile, experiments demonstrate that the phase transition is sluggish and kinetics is important in discerning the phase boundary. Additionally, the post-graphite phase appears to be superhard with hardness comparable to that of diamond.
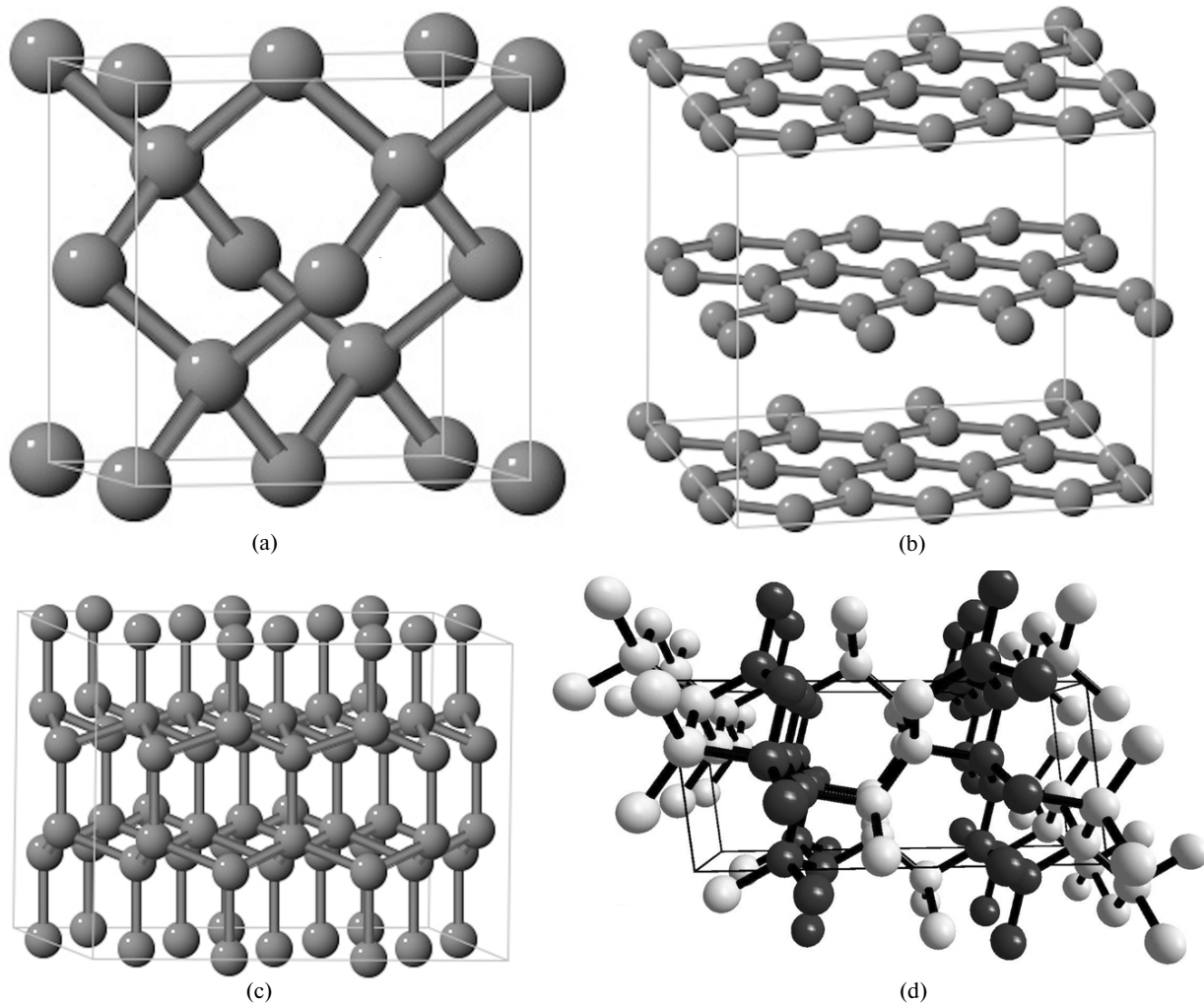
1. INTRODUCTION

From astronomy to mineralogy and zoology, carbon is one of the most important elements in nearly every field of science. Carbon is the fourth most abundant element by mass in the universe after hydrogen, helium, and oxygen [1]. The abundance of carbon along with its extraordinary ability to form diverse organic compounds under conditions commonly encountered on Earth makes carbon the essential basis for all known organic life. As such, carbon is the second most abundant element by mass in the human body, after oxygen [2]. Furthermore, carbon plays a critical role in many global issues: the carbon cycle is an integral part of climate change [3] as well as worldwide energy challenges [4].

Pure carbon exists in several forms with vastly different properties. Diamond is the most well-known form, as it is the hardest known naturally occurring material with the highest shear modulus (strongest resistance to fail under shear stress) [5]. In its pure form, diamond is a good conductor of heat, although being covalently bonded, diamond is a poor electrical conductor [6]. The diamond structure incorporates a network of covalent tetrahedral sp^3 bonds between atoms. Due to the high symmetry of this structure (Fig. 1a) and strength of the neighboring carbon bonds, diamond is extremely isotropic and transparent over wide ranges of the electromagnetic spectrum [6]. On the other hand, graphite exhibits properties remarkably different from diamond: graphite is opaque in appearance and is a semi-metal with highly anisotropic material properties. Graphite's hexagonal structure consists of parallel planes of covalent hexagonally sp^2 hybrid-bonded networks of carbon atoms layered in an AB sequence [7] (Fig. 1b). The layers in graphite are weakly bonded by van der Waals forces, and the anisotropy is the direct result of the difference between inter- and intra-planar bonding [8]. Along any direction parallel to the hexagonal planes (*a* and *b* axes), graphite is extremely hard, and conducts electricity and heat well [8]. Along the perpendicular direction (or *c*-axis), graphite is much more compressible, and has smaller thermal conductivity and larger electrical resistivity values. The electrical resistivity measured along the *c*-axis is ~10^2 to 10^5 times larger than that of the *a* axis [7]. All of these differences are attributed to the unique atomic bonding structures of planar sp^2 in graphite and three-dimensional sp^3 hybridization in diamond.

Fig. 1. Crystal structures of carbon. Diamond (a), graphite (b), hexagonal diamond (lonsdaleite) (c), and M-carbon (d). Figures (a)−(c) are reproduced from the U.S. Naval Research Laboratory website [70].

Graphite is the most stable phase of carbon under ambient conditions, while diamond is a metastable phase. However, because the driving force to transform diamond into graphite is small, the rate of the transition is negligible and thus, the diamond to graphite transition does not spontaneously occur at ambient conditions. The transition from graphite to diamond can occur only when subjected to high pressures and temperatures and usually a catalyst is required due to the slow kinetics [9]. For example, natural diamond is formed from carbon-bearing minerals buried in the Earth's upper mantle at pressures between 4.5 and 6 GPa (~135−185 km depth) and at temperatures between 900−1300°C [10]. Due to diamond's relative scarcity, desirable properties and beauty, it has long been treasured as a precious gemstone. The situation of diamond's scarcity changed when General Electric first synthesized diamond in the 1950s by duplicating the reaction conditions (high pressures and temperatures) of natural diamond in the Earth [9, 11]. With the increased yield, diamond has been extensively used and has generated revolutionary impacts in industry and science alike.

Although graphite and diamond are the most commonly known forms of carbon, under appropriate pressure and temperature conditions, there are several other forms of carbon. Hexagonal diamond, also known as lonsdaleite (Fig. 1c), has been found in carbon-rich meteorites, notably the Canyon Diablo iron meteorite [12], and is expected to have been formed in the high-pressure, high-temperature shock conditions of an impact, as inferred from laboratory measurements [13].
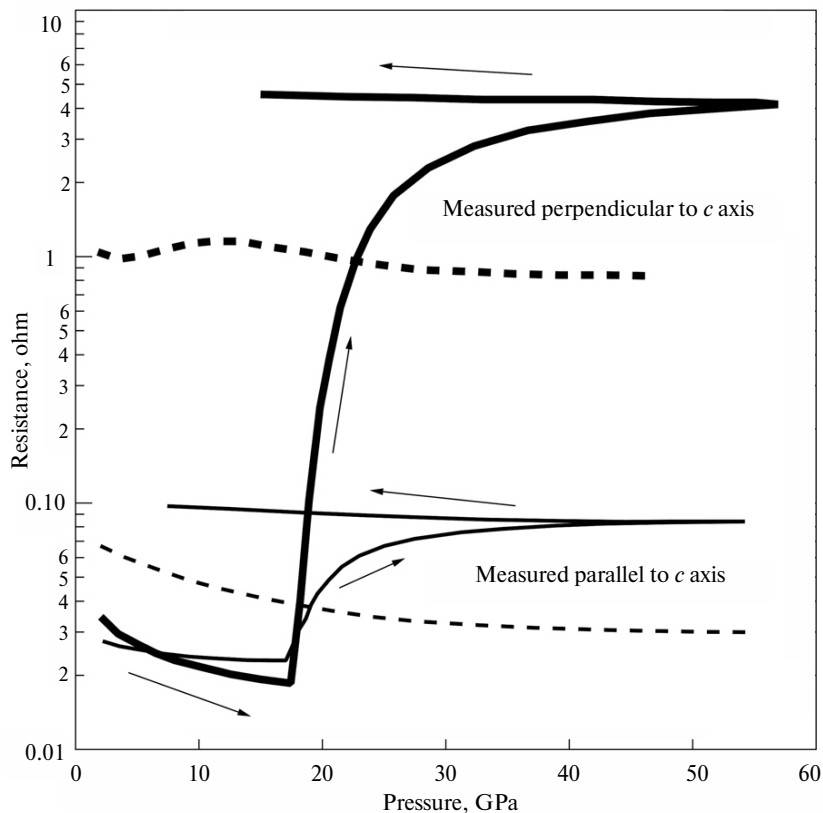
As graphite transforms into diamond (either cubic or hexagonal) under high-pressure and high-temperature conditions, straightforward questions naturally arise: what occurs if graphite is placed in a high-pressure environment without heating? Are diamond-like materials still produced? What is the post-graphite structure? What are its physical properties? How does its strength compare to diamond? Can it be synthesized more easily than diamond? Unlike the transition from graphite to diamond under high pressures and high temperatures, the cold-compressed behavior of graphite has been an enigma for over fifty years. In this review, a

detailed history of the study of graphite under high pressure and room temperature will be given, beginning with the observation of the pressure-induced phase transition in graphite through numerous characterization techniques, controversial identification of the high-pressure graphite phase, long-term efforts to solve this discrepancy, and securing an elegant solution to this enigma on the basis of comparison of experimental results with existing theoretical computations [e.g., 14, 15]. Further, the high-pressure room-temperature phase transition of graphite is sensitive to the form of the starting materials [16–18]. For this reason, we focus on crystalline hexagonal graphite, rather than amorphous graphite, fullerenes or carbon nanotubes. For a review of these carbon materials, please see the other sections in this special issue [19–21]. Additionally, there have been several reviews on the high-pressure, high-temperature behavior of carbon [22–25], however, in this review, we pay special attention to the long-standing controversies on the structural transitions of graphite at high pressures under room temperature conditions as shown through experiments.

2. HIGH-PRESSURE ROOM-TEMPERATURE PHASE TRANSITION

2.1. Resistivity Measurements

In 1962, Samara and Drickamer [26] first observed the room-temperature transition of graphite at approximately 10 GPa by measuring a jump in the resistivity, although this observation was not universal and depended on the nature of the starting material (powdered vs. pyrolytic) and along which axis the measurements were taken (*a* vs. *c*). Using a specifically-designed high-pressure electrical resistance cell [27] Aust and Drickamer [28] measured a large increase in resistance above ~17 GPa, measuring samples of single-crystal graphite oriented in both the *a* and *c* directions, respectively. At the transition, the *a*-axis resistance increased by more than two orders of magnitude, while the *c*-axis resistance increased by a factor of 4 (Fig. 2). The transition was observed only in single-crystal graphite samples, and was not observed in powdered graphite. Furthermore, this transition showed a large hysteresis: the resistance did not decrease again upon decompression to ~7 GPa, where data collection ceased.

Fig. 2. Resistance of graphite vs. pressure for single-crystal graphite (solid lines) and a pyrolytic graphite (dashed lines) as measured in both parallel (thin lines) and perpendicular (thick lines) orientations to the *c*-axis. The arrows denote the sequence of pressure paths. Note the large hysteresis in the data: the resistances do not revert to low-pressure values upon decompression, at least to pressures of ~15 and ~7 GPa in measurements perpendicular and parallel to the *c*-axis, respectively. Data reproduced from [28].

Soon after, another high-pressure phase identified as hexagonal diamond, or lonsdaleite (Fig. 1c), was investigated by Bundy and Kasper [13] while exploring the transition between graphite and diamond (see X-ray Diffraction section). Hexagonal diamond forms at temperatures greater than 1000°C and pressures higher than 13 GPa, implying that the phase found by Aust and Drickamer [28] was not lonsdaleite, and instead the phase partially synthesized by Aust and Drickamer has since been referred to as "cubic" graphite. In these studies, Bundy and Kasper [13] determined that chemical purity of the graphite samples did not matter, but crystalline order did: the transition occurred in well-ordered samples, but did not occur in poorly-ordered graphite, consistent with earlier measurements [28]. They also reported a similar hysteresis as observed by Aust and Drickamer [28], but ultimately observed a decrease in resistance upon depressurization below approximately 7 GPa.

Since then, several studies have been performed on cold-compressed graphite using a variety of high-pressure devices. In 1971, Okuyama et al. [29] performed room-temperature, high-pressure resistance measurements on graphite, but observed the transition in only a few samples: a synthetic sample annealed (prior to compression) to ~3500 K and a natural Madagascar sample at 17 and 16 GPa, respectively. The transition was not observed in synthetic samples annealed at temperatures less than ~3100 K at least up to pressures of ~25 GPa, suggesting that higher-temperature annealing induces higher order in synthetic samples. In 1994, Li and Mao [30] performed a series of high-pressure resistivity experiments in a multi-anvil press [31], where they measured polycrystalline graphite samples and amorphous carbon, and in a diamond-anvil cell [32] (DAC), where only graphite was measured. No transition was found in amorphous carbon, where order is lacking, but transitions similar to previous graphite experiments were seen in both the multi-anvil and DAC experiments at approximately 20 GPa. The DAC experiment also confirmed the previously observed hysteresis in the resistance behavior upon decompression [30].

Earlier studies focused on the abrupt increase in the resistance of graphite with increasing pressure as an indication of a phase transition and found varying transition pressures (~10−20 GPa) with a large hysteresis. However, more recently, resistivity measurements in a DAC have been used to study the kinetics of this phase transition looking at the rate of change in the resistance prior to, during, and following the transition both on compression and decompression at room temperature [33]. These long-duration experiments, completed over the course of tens of days to capture the sluggish behavior, pinned the phase transition of highly-ordered pyrolytic graphite (HOPG) to the post-graphite phase to occur at 19 ± 2 GPa with little hysteresis.
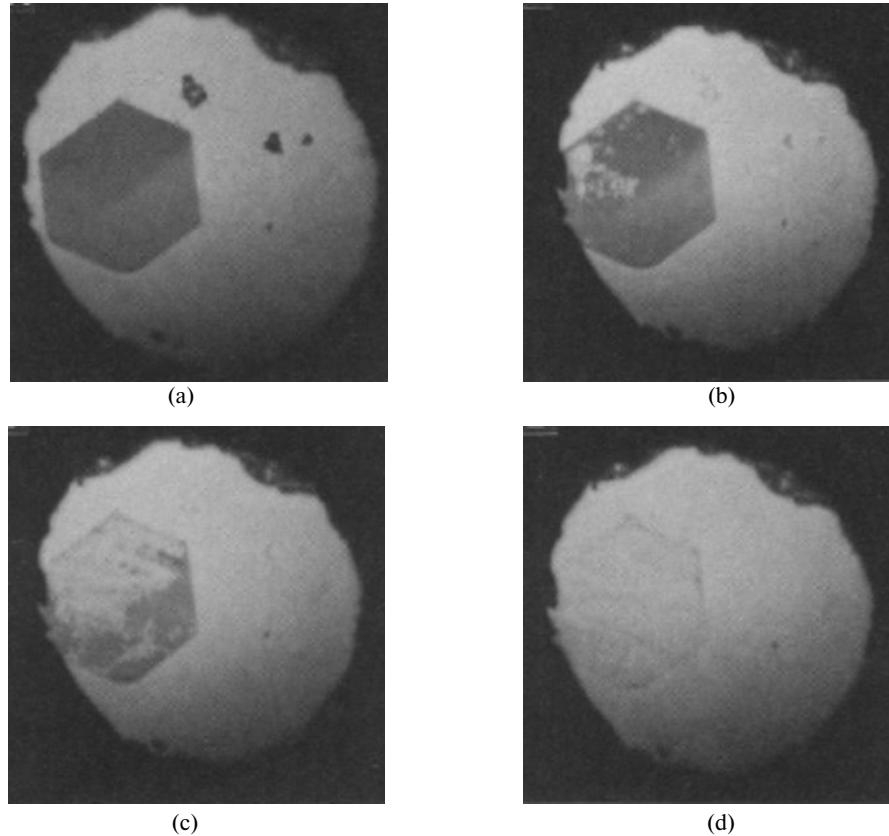
2.2. Optical Measurements

Another observation of the sluggishness of the phase transformation of graphite under high pressures was reported by Utsumi and Yagi [34], in which the starting material was a very thin (~1 μm in thickness) single crystal of graphite. This observation confirmed the first reports of transparency of high-pressure graphite given by earlier studies [35−37]. The Utsumi and Yagi [1991] sample was compressed in a DAC with a mixture of methanol and ethanol as the pressure medium, and the change of the transparency of the sample with pressure was studied through in situ optical microscopy (Fig. 3). Under compression, the sample did not exhibit any noticeable change until the pressure reached 18 GPa, at which a few light-transparent spots appeared in the sample. The presence of the transparent (i.e., decreased optical reflectivity) spots indicated the creation of a high-pressure phase inside the graphite sample, in agreement with previous results [38]. As the sample was kept at this pressure, more light-transparent spots appeared and spread across the whole sample chamber. After 2 hours, the entire sample became transparent. This transparent phase is only quenchable to room conditions if heated while at high pressure, thus becoming hexagonal diamond [13]. Otherwise, the unheated and transparent post-graphite phase reverts back to its original opaque character upon quench even if compressed to pressures as high as 50 GPa.

Although sample thickness was too large to see full transparency (~13 μm at the highest compressions), Montgomery et al. [33] also observed a reversion from transparent to opaque after decompression from pressures as high as ~28 GPa. Miller et al. [39] confirmed these room-temperature observations as well, but also found that the phase is quenchable at temperatures below 100 K, and proposed the mechanism behind the transition: a transfer of bonds from the graphite sp^2 hybrid bonds to the sp^3 hybrid bonds associated with diamond. This mechanism has been subsequently confirmed by inelastic X-ray scattering [40].
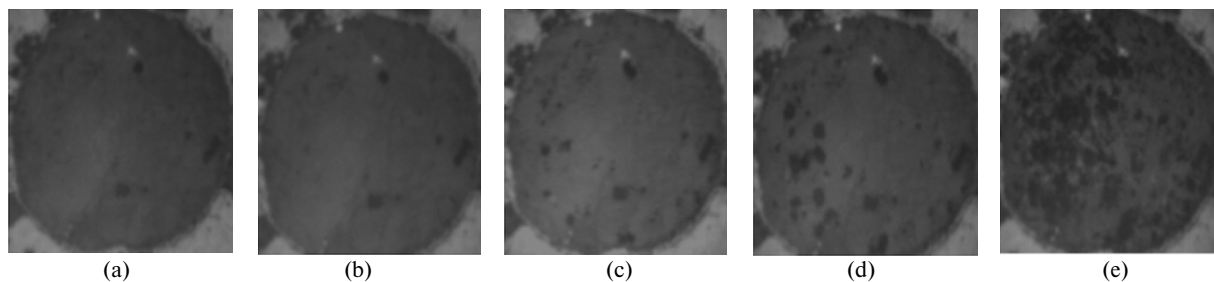
Recently, a new study was carried out to investigate the kinetics of the phase transition in HOPG [16]. The study found that at 19.8 GPa after 1 hour, a few dark spots appeared on the surface of sample while viewed under reflecting light, and with time the concentration of the dark spots increased (Fig. 4). After 93 hours at 19.8 GPa, most of the sample became dark. This observation is consistent with the previous observations of transparency of the post-graphite phase [34] (Fig. 3), and both reveal that the phase transition of graphite under cold compression is slow and requires a long time to complete the transition. In the more recent exper-

iment [16], although the sample did not become transparent, this is due to the increased thickness of the sample [34]. The earlier study had a thickness of ~1 micron as compared to the latter study thickness of at least an order of magnitude greater. In both cases, however, the once reflecting and electrically conducting material became insulating: the former became transparent and the latter became non-reflecting. Under high pressures, the new spots (whether transparent [34] or dark [16]) represent the nucleation and growth of the new phase and suggest that the high-pressure post-graphite phase is less conductive than graphite as demonstrated in other studies [36, 38].

These optical properties of graphite under high pressure reveal that the phase transition in graphite is sluggish and that long periods of time are needed to explore this phase transition.

(a)

(b)

(c)

(d)

Fig. 3. The evolution of light transmission through a thin single crystal of graphite at room temperature over an extended period of time. The starting sample at ambient pressure (a). At 18 GPa, the transparent spots appear in the sample (b). After 30 minutes with pressure held at 18 GPa, more transparent spots accumulate across the sample area (c). After 2 hours, the whole sample transforms into a new phase with high light transparency (d). Reproduced from [34].

(a)   (b)   (c)   (d)   (e)

Fig. 4. Phase evolution of compressed graphite vs. relaxation time. Photomicrographs (a) and (b) taken immediately at pressures of 6.9 and 19.8 GPa, respectively. The dark spots in (a) and (b) are from ruby chips. Images (c–e) captured at a pressure of 19.8 GPa after relaxation times of 1, 51, and 93 hours, respectively. Figure reproduced from [16].

2.3. Spectroscopy

There have been several spectroscopic studies of graphite under high-pressure conditions, which, however, are limited to DAC or gem–anvil cell (GAC) [41] experiments. DAC studies are limited due to the large signal

from the diamond anvils themselves and overlap with potential signal from the post-graphite phase. Graphite has a characteristic Raman peak at ~1581 cm^{-1} ("G" band) at ambient conditions. With increasing pressures, this peak shifts to higher wavenumbers and broadens [35, 37, 41–44], effectively disappearing at high pressures [16]. Using a GAC, specifically equipped with sapphire anvils, Xu et al. [41] confirmed that high-pressure phase transition in graphite occurs, however, the Raman spectra were not conducive to either hexagonal or cubic diamond. Upon quenching to room temperature, the G band returns along with broad D and D′ bands at ~1350 and ~1620 cm^{-1}, respectively [16] consistent with a reversion to sub-micron sized graphite particles [45–47], suggesting that the post-graphite phase transition causes a grain size reduction [16].

2.4. X-ray Diffraction

The high symmetry of graphite (hexagonal, $P6_3/mmc$) and comparably soft nature yield sharp and intense X-ray diffraction (XRD) peaks despite the low-Z character of carbon. As such, there are several XRD studies of graphite under pressure that show the highly anisotropic nature of hexagonal graphite [42, 48–50]: the c-axis is approximately 35 times more compressible than the a-axis (Table 1).

Table 1. The lattice parameters and volume per atom in graphite, as well as the corresponding Birch-Murnaghan equation of state (EOS) parameters, assuming $K_{0x}' = 4$ are listed. Uncertainties are given in parentheses. Note that for H-graphite, $K_{0a} \gg K_{0c}$, is indicative of the highly anisotropic nature of graphite
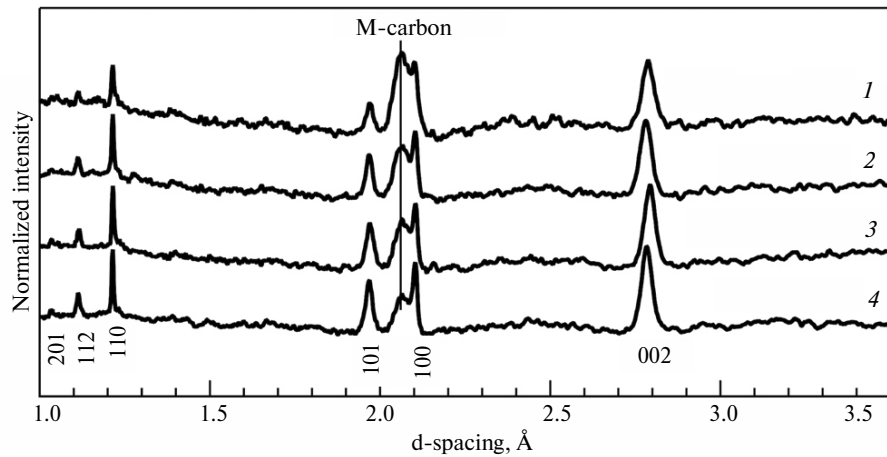
a_0, Å	K_{0a}, GPa	c_0, Å	K_{0c}, GPa	V_0, Å^3	K_0, GPa	Reference
2.462 (0.001)	442 (6)	6.721 (0.002)	12.0 (0.1)	8.817 (0.011)	57.3 (0.8)	[16]
2.461 (NA)	516 (41)	6.708 (NA)	14.9 (0.5)	8.797 (NA)	67.4 (3.8)	[50]
2.459 (0.004)	481 (32)	6.706 (0.003)	11.9 (0.1)	8.78 (0.01)	51.2 (1.4)	[42]
2.462 (NA)	449.7 (5.1)	6.707 (NA)	13.1 (0.3)	8.802 (NA)	59.6 (1.1)	[48]

The first XRD measurement attempts of the post-graphite phase yielded an interpretation of a cubic structure [28] for a sample synthesized at high pressure and room temperature and quenched to room temperatures. Since then, the cubic structure has not been reproduced and the initial identification was likely spurious [13]. Additionally, the room-temperature high-pressure post-graphite phase has not been measured upon quench and all samples heated to temperatures less than ~1300 K, revert back to graphite (e.g., [13, 16, 38, 42]).
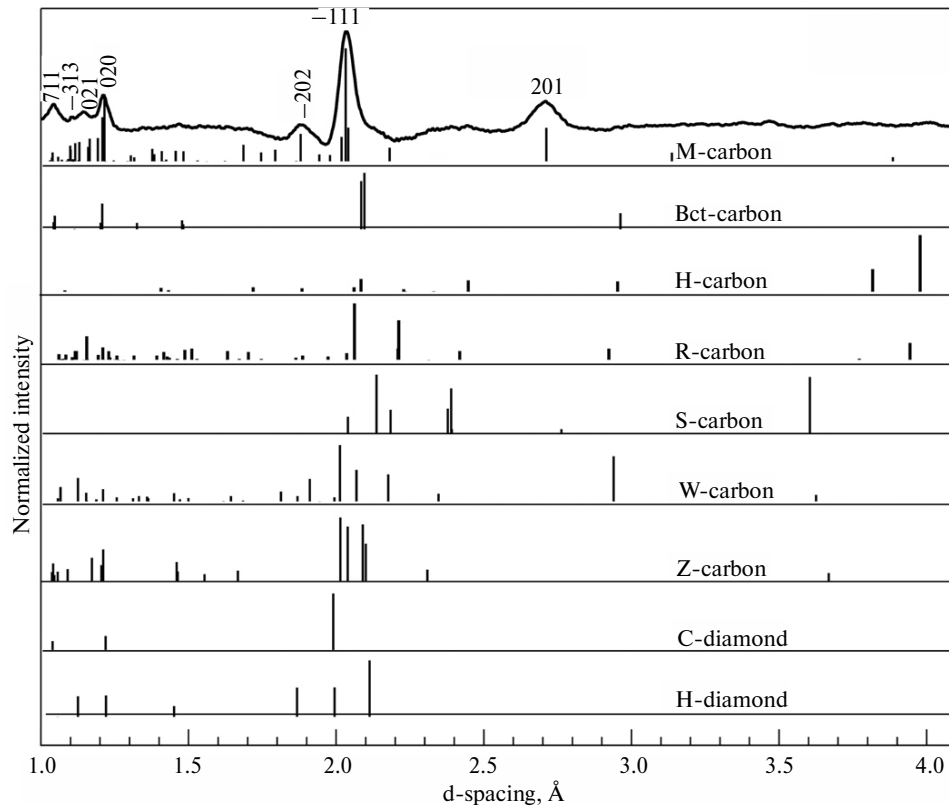
In 1966, Lynch and Drickamer [50], conducted XRD measurements on graphite and found the phase transition at ~16 GPa, where the compressibility of the a-axis of graphite became stiffer than diamond. In 1989, Hanfland et al. [42] measured the XRD of graphite and found that above ~14 GPa, a phase transition occurred but the XRD pattern quality became too poor to be able to identify a structure. Soon after, Zhao and Spain [48], found similar results, although with the phase transition occurring at a slightly lower pressure of ~11 GPa.

With the advent of synchrotron radiation and the increased X-ray flux, the hopes of identifying the structure of the post-graphite phase were renewed. Rather than taking 5–15 days to collect a single XRD pattern with an X-ray laboratory source [48], the intense early synchrotron sources provided sufficient flux so that measurement times dropped to 10s of minutes to hours [49, 51]. Even so, the structure remained elusive.

More recently, there have been two studies [16, 40], which have measured the XRD of the post-graphite phase with modern synchrotron sources with increased flux and monochromatic energy. The first of these studies [40] spurred numerous theoretical studies to predict the nature of the new structure and yielded more than 9 candidate structures: bct-C$_4$ [52], H- [53], K$_4$- [54], M- [55, 56], R- [57], S- [53] T- [58], W- [59], Z-carbon [60], and other Z-series carbon polymorphs [61]. For a complete review of the structures and respective energetics, please see the review article in this Special Issue [14, 15]. Wang et al. [16] waited a long time (at least 6 hours to as long as 1 year) between XRD pattern collections due to the sluggish nature of the transition (Fig. 5). Patience yielded quality XRD patterns that allowed discrimination between the numerous predictions (Fig. 6). From the long-duration patterns, the M-carbon structure was found to be the most consistent structure (Fig. 1d), as compared with every other predicted structure [16].

Fig. 5. XRD patterns collected at pressures of 24.9 and 26.3 GPa immediately as well as after 9 and 6.3 hours, respectively: (*1*) 26.1 GPa, 6.3 h; (*2*) 26.3 GPa; (*3*) 24.6 GPa, 9 h; (*1*) 24.9 GPa. The increase of the intensity of (−111) peak, the strongest peak of M-carbon and identified by the near vertical line near 2 Å, suggests that the concentration of M-carbon increases with relaxation time, confirming that the phase transformation from graphite to M-carbon is sluggish. Reproduced from [16].

Fig. 6. XRD pattern at ~50 GPa and corresponding predicted XRD peaks for M-carbon (*hkl*'s used to determine volume are labeled), bct-C$_4$ [52], H-carbon [53], R-carbon [57], S-carbon [53], W-carbon [59], Z-carbon [60], cubic diamond (C-diamond) [71] and hexagonal diamond (H-diamond) [72] are shown as vertical lines. Figure reproduced from [16].

3. MECHANICAL PROPERTIES

3.1. Equation of State

The EOS of a solid gives the relationship between volume and pressure. One such EOS developed by Birch [62], building upon the work of Murnaghan [63], is derived from the theory of finite strain and works well for most solid materials. The third-order Birch-Murnaghan EOS [62, 64] is given by:

$$P = 3f(1 + 2f)^{5/2} K_0 \left(1 + f\left(\frac{3}{2}K_0' - 6\right)\right),$$

where $f = \frac{1}{2}\left[\left(\frac{V}{V_0}\right)^{-2/3} - 1\right]$.

V_0 and V are the unit-cell volumes at ambient and high-pressure conditions, respectively, and K_0 and K_0' are ambient isothermal bulk modulus and its pressure derivative, respectively. A second-order Birch-Murnaghan EOS occurs when K_0' is set to a value of 4, thus truncating the pressure relationship. The lattice parameters can also be fit individually to a Birch-Murnaghan-like formulism by replacing V and V_0 with a^3 and a_0^3, b^3 and b_0^3, and c^3 and c_0^3 respectively, yielding each a linear modulus K_{0a}, K_{0b} and K_{0c}, with corresponding pressure derivatives K_{0a}', K_{0b}' and K_{0c}' [65]. The bulk modulus is a measure of how incompressible a material is.
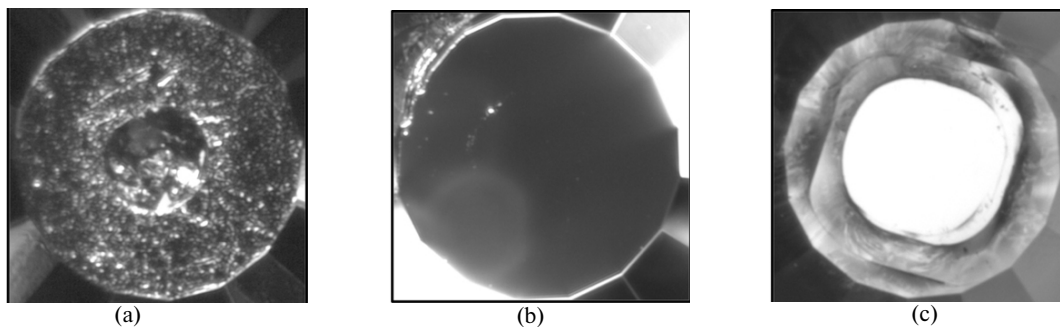
The equation of state of H-graphite has been determined experimentally by using synchrotron XRD coupled with DAC [16, 42, 48, 50, 66] and large volume high-pressure apparatuses [50] (Table 1). Numerous theoretical computations have been conducted to characterize the mechanical properties of M-carbon, but only one set of experimental data is available thus far to validate the predictions [16]. Nevertheless, both experiment and computations show that M-carbon has extremely low compressibility comparable to other stiff materials such as cubic-BN (387 ± 4 GPa) [67] and ReB_2 (334 ± 23 GPa) [68] (Table 2). Additionally, like graphite, M-carbon also shows anisotropy in compressibility along lattice axes a, b, and c, although to a lesser extent than graphite.

Table 2. Experimental and theoretical values for lattice parameters and volume/atom in M-carbon as well as the corresponding Birch-Murnaghan EOS parameters. Uncertainties are given in parentheses. Where values are not available or given, NA is noted

a, Å	K_{0a}, GPa	b, Å	K_{0b}, GPa	c, Å	K_{0c}, GPa	β, deg	V_0, Å³	K_0, GPa	K_0'	Method	Reference
9.123 (0.001)	527 (2)	2.559 (0.001)	271 (1)	4.088 (0.001)	267 (1)	97.38 (0.79)	5.86 (0.01)	368 (1)	4	Experiment, DAC	[16]
9.089 (NA)	NA	2.496 (NA)	NA	4.104 (NA)	NA	96.96 (NA)	5.78 (NA)	431.2 (NA)	NA	Theory, LDA	[55]
NA	NA	NA	NA	NA	NA	NA	5.991 (NA)	398 (NA)	3.61	Theory, GGA	[72]
NA	NA	NA	NA	NA	NA	NA	5.745 (NA)	422 (NA)	3.77	Theory, LDA	[72]

3.2. Mechanical Strength

Although graphite, in its natural state, is a soft material, once transformed to its cold-compressed structure, it becomes superhard with the capacity to indent the diamond anvils at relatively low pressures (< 30 GPa) [16, 40]. Upon quenching the sample to ambient conditions and opening the DAC, cracks along the sample boundary were observed on the diamond culets. The damage to the anvils correlates with the highest pressures reached during the measurements (Fig. 7). At 32 GPa, only a microcrack was left on the anvil's surface; how-

(a)   (b)   (c)

Fig. 7. Photomicrographs of diamond anvils after experiencing various high-pressure conditions. The culets are 300 μm in diameter. (a) Image of the gasket filled with HOPG prior to compression. (b) Slightly scratched surface of diamond after reaching a maximum pressure of 32 GPa. The photomicrograph was taken with reflected light. (c) Badly fractured anvil by M-carbon after reaching a maximum pressure of 50 GPa. The image was taken with transmitted light. Reproduced from [16].

ever, after compression to 50 GPa, the anvils were severely fractured. These observations suggest that M-carbon has super strength and hardness rivaling that of diamond, and is capable of deforming and indenting the diamond when the two materials are pressed against each other under nominal compression. One parameter to evaluate a material's strength is its hardness, however, M-carbon has not been recovered at ambient conditions, thus a hardness measurement is lacking. However, the hardness obtained from theoretical computations (83.1 GPa [55], 91.5 GPa [58]) suggest that this high-pressure graphite phase is a superhard material.

4. CONCLUSIONS

Although carbon may appear simple and common, it is indeed, non-trivial and often leads to controversial results even when investigated with state-of-the-art computational and experimental methods. The history of graphite under high pressures is replete with disputes and controversies. Although the phase transition of graphite under cold compression has been observed by a series of experimental approaches, largely due to its complicated chemistry, detailed and accurate information regarding the room-temperature high-pressure graphite phase was unknown for a long time. After more than fifty years of effort, major progress has been achieved with the identification of the crystal structure of the post-graphite phase, namely M-carbon, which was predicted by theoretical computations [55] and later confirmed by XRD measurements [16]. This newly-identified phase has the extraordinary ability to damage diamond, however, its unquenchable nature makes ex-situ measurements, for example, hardness measurements, very challenging. Therefore, although we have reached a milestone in the study of graphite by confirming the crystal structure of the post-graphite phase, we should keep in mind that many of its properties remain enigmatic and thus it may be awhile before the strengths of M-carbon are realized in science or industry. Among the many technical difficulties, one basic requirement for the eventual application of M-carbon is the ability to stabilize it at ambient conditions. Additionally, as kinetics appear to be very important in the room-temperature post-graphite transition, the nature of the synthesis conditions and starting material may also affect the manufacture of metastable phases. However, the kinetics of the transition to M-carbon has been recently found to be more favorable than the same transition of graphite to either diamond, bct-C_4, W-carbon or other sp^3 forms of carbon [69].

5. ACKNOWLEDGEMENTS

REFERENCES

1. Caroll, B. and Ostlie, D., *An Introduction to Modern Astrophysics*, San Francisco, California: Benjamin-Cummings Publishing Company, 2007.
2. Harper, H.A., Rodwell, V.W., and Mayes, P.A., *Review of Physiological Chemistry*, Los Altos, California: Lange Medical Publications, 1977, p. 681.
3. Cao, M. and Woodward, F.I., Dynamic Responses of Terrestrial Ecosystem Carbon Cycling to Global Climate Change, *Nature*, 1998, vol. 393, no. 6682, pp. 249–252.
4. Brown, M.A., Levine, M.D., Short, W., and Koomey, J.G., Scenarios for a Clean Energy Future, *Energy Policy*, 2001, vol. 29, no. 14, pp. 1179–1196.
5. Neves, A.J. and Nazaré, M.H., *Properties, Growth and Applications of Diamond*, London, UK: Institution of Engineering and Technology, 2001, pp. 142–147.
6. Pan, L. and Kania, D., *Diamond: Electronic Properties and Applications*, Boston: Kluwer 1995.
7. Chung, D.D.L., Review Graphite, *J. Mater. Sci.*, 2002, vol. 37, no. 8, pp. 1475–1489.
8. Pierson, H.O., *Handbook of Carbon, Graphite, Diamond and Fullerenes*, Park Ridge, New Jersey: Noyes Publications, 1993.
9. Bovenkerk, H.P., Bundy, F.P., Hall, H.T., Strong, H.M., and Wentorf, R.H., Preparation of Diamond, *Nature*, 1959, vol. 184, no. 4693, pp. 1094–1098.
10. Carlson, R.W., *The Mantle and Core*, New York: Elsevier, 2005, p. 248.
11. Bundy, F.P., Hall, H.T., Strong, H.M., and Wentorf, R.H., Jr., Man-Made Diamonds, *Nature*, 1955, vol. 176, no. 4471, pp. 51–55.
12. Frondel, C. and Marvin, U.B., Lonsdaleite, a Hexagonal Polymorph of Diamond, *ibid.*, 1967, vol. 214, no. 5088, pp. 587–589.
13. Bundy, F.P. and Kasper, J.S., Hexagonal Diamond–A New Form of Carbon, *J. Chem. Phys.*, 1967, vol. 46, no. 9, pp. 3437–3446.
14. Boulfelfel, S.E., Zhu, Q., and Oganov, A.R., Novel sp^3-Forms of Carbon Predicted by Evolutionary Metadynamics and Analysis of Their Synthesizability Using Transition Path Sampling, *J. Superhard Mater.*, 2012, vol. 34, no. 6, pp. 350–359.

15. He, C., Sun, L.Z., and Zhong, J., Prediction of Superhard Carbon Allotropes from a Segment Combination Method, *ibid.*, 2012, vol. 34, no. 6, pp. 386–399.

16. Wang, Y., Panzik, J.E., Kiefer, B., and Lee, K.K.M., Crystal Structure of Graphite Under Room-Temperature Compression and Decompression, *Sci. Reports*, 2012, vol. 2, art. 520.

17. Lin, Y., Zhang, L., Mao, H.K., Chow, P., Xiao, Y., Baldini, M., Shu, J. and Mao, W.L., Amorphous Diamond: A High-Pressure Superhard Carbon Allotrope, *Phys. Rev. Lett.*, 2011, vol. 107, no. 17, art. 175504.

18. Wang, Z., Zhao, Y., Tait, K., Liao, X., Schiferl, D., Zha, C., Downs, R.T., Qian, J., Zhu, Y. and Shen, T., A Quenchable Superhard Carbon Phase Synthesized by Cold Compression of Carbon Nanotubes, *PNAS*, 2004, vol. 101, no. 3, pp. 13699–13703.

19. Brazhkin, V.V. and Lyapin, A.G., Hard and Superhard Carbon Phases Synthesized from Fullerites under Pressure, *J. Superhard Mater.*, 2012, vol. 34, no. 6, pp. 400–423.

20. Kurio, A., Tanaka, Y., Sumiya, H., Irifune, T., Shinmei, T., Ohfuji, H. and Kagi, H., Wear Resistance of Nano-Polycrystalline Diamond with Various Hexagonal Diamond Contents, *ibid.*, 2012, vol. 34, no. 6, pp. 343–349.

21. Zhao, Z., Zhou, X.-F., Hu, M., Yu, D., He, J., Wang, H.-T., Tian, Y. and Xu, B., High-Pressure Behaviors of Carbon Nanotubes, *ibid.*, 2012, vol. 34, no. 6, pp. 371–385.

22. Bundy, F.P., The *p, T* Phase and Reaction Diagram for Elemental Carbon, 1979, *J. Geophysical Res.*, 1980, vol. 85, no. B12, pp. 6930–6936.

23. Clarke, R. and Uher, C., High-Pressure Properties of Graphite and Its Intercalation Compounds, *Adv. Phys.*, 1984, vol. 33, no. 5, pp. 469–566.

24. Bundy, F.P., Bassett, W.A., Weathers, M.S., Hemley, R.J., Mao, H.K., and Goncharov, A.F., Review Article: The Pressure-Temperature Phase and Transformation Diagram for Carbon; Updated through 1994, *Carbon*, 1996, vol. 34, no. 2, pp. 141–153.

25. Badding, J.V. and Lueking, A.D., Reversible High Pressure sp^2-sp^3 Transformations in Carbon, *Phase Transitions*, 2007, vol. 80, nos. 10–12, pp. 1033–1038.

26. Samara, G.A. and Drickamer, H.G., Effect of Pressure on Resistance of Pyrolytic Graphite, *J. Chem. Phys.*, 1962, vol. 37, no. 3, pp. 471–474.

27. Balchan, A.S. and Drickamer, H.G., High Pressure Electrical Resistance Cell, and Calibration Points above 100 Kilobars, *Review of Scientific Instruments*, 1960, vol. 32, no. 3, pp. 308–313.

28. Aust, R.B. and Drickamer, H.G., Carbon—A New Crystalline Phase, *Science*, 1963, vol. 140, no. 3568, pp. 817–819.

29. Okuyama, N., Yasunaga, H., Minomura, S., and Takeya, K., Dependence of the Resistance on Pressure in the *c*–Direction of Pyrolytic and Natural Graphite, *Jpn. J. Appl. Phys.*, 1971, vol. 10, no. 11, pp. 1645–1646.

30. Li, X. and Mao, H.K., Solid Carbon at High Pressure: Electrical Resistivity and Phase Transition, *Phys. Chem. Minerals*, 1994, vol. 21, no. 1, pp. 1–5.

31. Liebermann, R. and Wang, Y., Characterization of Sample Environment in a Uniaxial Split-Sphere Apparatus, in *High-Pressure Research: Application to Earth and Planetary Sciences*, Syono, Y. and Manghnani, M.N., Eds., Washington, DC: Am. Geophys. Un., 1992, pp. 19–31.

32. Mao, H.K. and Bell, P.M., *Techniques of Electrical Conductivity Measurement to 300 Kbar*, New York, United States: Academic, 1977, pp. 493–502.

33. Montgomery, J.M., Kiefer, B. and Lee, K.K.M., Determining the High-Pressure Phase Transition in Highly-Ordered Pyrolitic Graphite with Time–Dependent Resistance Measurements, *J. Appl. Phys.*, 2011, vol. 110, no. 4, art. 043725.

34. Utsumi, W. and Yagi, T., Light-Transparent Phase Formed by Room-Temperature Compression of Graphite, *Science*, 1991, vol. 252, no. 5012, pp. 1542–1544.

35. Goncharov, A.F., Makarenko, I.N., and Stishov, S.M., Graphite at Pressures up to 55 GPa: Optical Properties and Raman Spectra, *High Press. Res.*, 1990, vol. 4, nos. 1–6, pp. 345–347.

36. Goncharov, A.F., Makarenko, I.N., and Stishov, S.M., Graphite at Pressures up to 55 GPa: Optical Properties and Raman Scattering—Amorphous Carbon? *Sov. Phys. JETP*, 1989, vol. 69, no. 2, pp. 380–381.

37. Goncharov, A.F., Observation of Amorphous Phase of Carbon at Pressures above 23 GPa, *JETP Lett.*, 1990, vol. 51, no. 7, pp. 418–421.

38. Hanfland, M., Syassen, K., and Sonnenschein, R., Optical Reflectivity of Graphite under Pressure, *Phys. Rev. B*, 1989, vol. 40, no. 3, pp. 1951–1954.

39. Miller, E.D., Nesting, D.C. and Badding, J.V., Quenchable Transparent Phase of Carbon, *Chem. Mater.*, 1997, vol. 9, no. 1, pp. 18–22.

40. Mao, W.L., Mao, H., Eng, P.J., Trainor, T.P., Newville, M., Kao, C., Heinz, D.L., Shu, J., Meng, Y. and Hemley, R.J., Bonding Changes in Compressed Superhard Graphite, *Science*, 2003, vol. 302, no. 5644, pp. 425–427.

41. Xu, J., Mao, H. and Hemley, R., The Gem Anvil Cell: High-Pressure Behavior of Diamond and Related Materials, *J. Phys: Condens. Matter*, 2002, vol. 14, no. 44, pp. 11549–11552.

42. Hanfland, M., Beister, H., and Syassen, K., Graphite under Pressure: Equation of State and First-Order Raman Modes, *Phys. Rev. B*, 1989, vol. 39, no. 17, pp. 12598–12603.

43. Liu, Z., Wang, L., Zhao, Y., Cui, Q. and Zou, G., High-Pressure Raman Studies of Graphite and Ferric Chloride-Graphite, *J. Phys.: Condens. Matter*, 1990, vol. 2, no. 40, pp. 8083–8088.

44. Schindler, T. and Vohra, Y.K., A Micro-Raman Investigation of High-Pressure Quenched Graphite, *ibid.*, 1995, vol. 7, no. 47, pp. L637–L642.

45. Loa, I., Moschel, C., Reich, A., Assenmacher, W., Syassen, K., and Jansen, M., Novel Graphitic Spheres: Raman Spectroscopy at High Pressures, *Phys. Stat. Sol. (b)*, 2001, vol. 223, no. 1, pp. 293–298.

46. Pocsik, I., Hundhausen, M., Koos, M., and Ley, L., Origin of the D Peak in the Raman Spectrum of Microcrystalline Graphite, *J. Non-Cryst. Solids*, 1998, vol. 227–230, no. 2, pp. 1083–1086.

47. Ferrari, A.C. and Robertson, J., Interpretation of Raman Spectra of Disordered and Amorphous Carbon, *Phys. Rev. B*, 2000, vol. 61, no. 20, pp. 14095–14107.

48. Zhao, Y.X. and Spain, I.L., X-ray Diffraction Data for Graphite to 20 GPa, *ibid.*, 1989, vol. 40, no. 2, pp. 993–997.

49. Yagi, T., Utsumi, W., Yamakata, M., Kikegawa, T., and Shimomura, O., High-Pressure in situ X-ray Diffraction Study of the Phase Transfromation from Graphite Pyrolitic to Hexagonal Diamond at Room Temperature, *ibid.*, 1992, vol. 46, no. 10, pp. 6031–6039.

50. Lynch, R.W. and Drickamer, H.G., Effect of High Pressure on the Lattice Parameters of Diamond, Graphite, and Hexagonal Boron Nitride, *J. Chem. Phys.*, 1966, vol. 44, no. 1, pp. 181–184.

51. Kim, Y. and Na, K., High Pressure X-Ray Diffraction Study on a Graphite Using Synchrotron Radiation, *J. Petrol. Soc. Korea*, 1994, vol. 3, no. 1, pp. 34–40.

52. Umemoto, K., Wentzcovitch, R.M., Saito, S., and Miyake, T., Body-Centered Tetragonal C4: A Viable sp^3 Carbon Allotrope, *Phys. Rev. Lett.*, 2010, vol. 104, no. 12, art. 125504.

53. He, C., Sun, L.Z., Zhang, C.X., Zhang, K.W., Peng, X., and Zhong, J., New Superhard Carbon Phases Between Graphite and Diamond, *Solid State Comm.*, 2012, vol. 152, no. 16, pp. 1560–1563.

54. Itoh, M., Kotani, M., Naito, H., Sunada, T., Kawazoe, Y., and Adschiri, T., New Metallic Carbon Crystal, *Phys. Rev. Lett.*, 2009, vol. 102, no. 5, art. 055703.

55. Li, Q., Ma, Y., Oganov, A.R., Wang, H., Wang, H., Xu, Y., Cui, T., Mao, H.K., and Zou, G., Superhard Monoclinic Polymorph of Carbon, *ibid.*, 2009, vol. 102, no. 17, art. 175506.

56. Oganov, A.R. and Glass, C.W., Crystal Structure Prediction Using Ab Initio Evolutionary Techniques: Principles and Applications, *J. Chem. Phys.*, 2006, vol. 124, no. 24, art. 244704.

57. Niu, H., Chen, X., Wang, S., Li, D., Mao, W.L. and Li, Y., Families of Superhard Crystalline Carbon Allotropes Constructed via Cold Compression of Graphite and Nanotubes, *Phys. Rev. Lett.*, 2012, vol. 108, no. 13, art. 135501.

58. Sheng, X.L., Yan, Q.B., Ye, F., Zheng, Q.R., and Su, G., T-Carbon: A Novel Carbon Allotrope, *ibid.*, 2011, vol. 106, no. 15, art. 155703.

59. Wang, J.T., Chen, C., and Kawazoe, Y., Low-Temperature Phase Transformation from Graphite to sp^3 Orthorhombic Carbon, *ibid.*, 2011, vol. 106, no. 7, art. 075501.

60. Amsler, M., Flores-Livas, J.A., Lehtovaara, L., Balima, F., Ghasemi, S.A., Machon, D., Pailhès, S., Willand, A., Caliste, D., Botti, S., Miguel, A.S., Goedecker, S., and Marques, M.A.L., Crystal Structure of Cold Compressed Graphite, *ibid.*, 2012, vol. 108, no. 6, art. 065501.

61. Wang, J.T., Chen, C.F., and Kawazoe, Y., Orthorhombic Carbon Allotrope of Compressed Graphite: Ab Initio Calculations, *Phys. Rev. B*, 2012, vol. 85, no. 3, art. 033410.

62. Birch, F., Finite Strain Isotherm and Velocities for Single-Crystal and Polycrystalline NaC1 at High Pressures and 300 K, *J. Geophys. Res.*, 1978, vol. 83, no. B3, pp. 1257–1268.

63. Murnaghan, F.D., Finite Deformations of an Elastic Solid, *Amer. J. Math.*, 1937, vol. 59, no. 2, pp. 235–260.

64. Jeanloz, R., Finite-Strain Equation of State for High-Pressure Phases, *Geophys. Res. Lett.*, 1981, vol. 8, no. 12, pp. 1219–1222.

65. Xu, H., Zhao, Y., Zhang, J., Wang, Y., Hickmott, D.D., Daemen, I.I., Hartl, M.A., and Wang, L., Anisotropic Elasticity of Jarosite: A High-P Synchrotron XRD Study, *Am. Mineral.*, 2010, vol. 95, no. 1, pp. 19–23.

66. Nakayama, A., Iijima, S., Koga, Y., Shimizu, K., Hirahara, K., and Kokai, F., Compression of Polyhedral Graphite up to 43 GPa and X-Ray Diffraction Study on Elasticity and Stability of the Graphite Phase, *Appl. Phys. Lett.*, 2004, vol. 84, no. 25, pp. 5112–5114.

67. Goncharov, A.F., Crowhurst, J.C., Dewhurst, J.K., Sharma, S., Sanloup, C., Gregoryanz, E., Guignot, N., and Mezouar, M., Thermal Equation of State of Cubic Boron Nitride: Implications for a High-Temperature Pressure Scale, *Phys. Rev. B*, 2007, vol. 75, no. 22, art. 224114.

68. Wang, Y., Zhang, J., Daemen, L.L., Lin, Z., Zhao, Y. and Wang, L., Thermal Equation of State of Rhenium Diboride by High Pressure-Temperature Synchrotron X-Ray Studies, *ibid.*, 2008, vol. 78, no. 22, art. 224106.

69. Boulfelfel, S.E., Oganov, A.R., and Leoni, S., Understanding the Nature of "Superhard Graphite", *Sci. Rep.*, 2012, vol. 22, art. 471.

70. NRL, The Diamond (A4) Crystal Structure, 2008.

71. Occelli, F., Loubeyre, P., and Letoullec, R., Properties of Diamond under Hydrostatic Pressures up to 140 GPa, *Nature Mater.*, 2003, vol. 2, no. 3, pp. 151–154.

72. Liang, Y., Zhang, W., and Chen, L., Phase Stabilities and Mechanical Properties of Two New Carbon Crystals, *EPL,* 2009, vol. 87, no. 5, art. 56003.